

Signatures of mechanosensitive gating

R. G. Morris

National Centre for Biological Sciences, Tata Institute for Fundamental Research, GKVK,
Bellary Road, Bangalore, 560064, INDIA.

Abstract

The question of how mechanically-gated membrane channels open and close is notoriously difficult to address, especially if the protein structure is not available. This perspective highlights the relevance of micropipette-aspirated single-particle tracking— used to obtain a channel’s diffusion coefficient, D , as a function of applied membrane tension, σ — as an indirect assay for determining functional behaviour in mechanosensitive channels. Whilst ensuring that the protein remains integral to the membrane, such methods can be used to identify not only the gating mechanism of a protein, but also associated physical moduli, such as torsional- and dilational-rigidity, which correspond to the protein’s effective shape change. As an example, three distinct D versus σ “signatures” are calculated, corresponding to gating by dilation, gating by tilt, and a combination of both dilation and tilt. Both advantages and disadvantages of the approach are discussed.

Submitted [DATE], and accepted for publication [DATE].

*Correspondence: richardgm@ncbs.res.in.

Address reprint requests to Richard G. Morris, National Centre for Biological Sciences, Tata Institute for Fundamental Research, GKVK, Bellary Road, Bangalore, 560064, India. Tel.:+91 80 2366 6001, ext. 6060.

Editor: [INSERT].

INTRODUCTION

The importance of mechanically gated membrane channels was underlined recently following the discovery of the *Piezo* family of proteins: mammalian counterparts to the well studied membrane channels found in invertebrates (1–8). However, the mechanism by which these channels open and close is not yet fully understood. The state of the art, which has been successful in the study of ion channels and pumps, is to infer functional properties from the protein’s structure, found via X-ray crystallography (9–14) or (single particle) cryo-electron microscopy (15, 16). Due the complexity of such techniques, each has certain limitations. For the former, crystallizing membrane proteins is fraught with difficulty, despite recent advances (17–19). For the latter, resolution can be an issue, leading to ambiguity of certain structural details. In both cases, proteins are typically isolated from their natural membrane environment via chemical modification (20) (although so-called surfactant-free techniques— whereby a protein is isolated in a co-polymer solvated membrane nanodisc (21, 22)— are a maturing field which may provide an alternative method of purification). Moreover, once a protein structure has been obtained, attempting to infer

a gating mechanism is somewhat subjective, particularly in the case of mechanosensitive channels, which rely less on the careful positioning of localized charge residues than, for example, voltage-gated channels.

In the absence of structural data, or to mitigate the aforementioned issues with a complimentary assay, an *indirect* method is required, where the protein exists in its natural environment of a tension-bearing lipid bilayer membrane. For this to be possible, the conformational changes which occur during gating must leave a distinct signature in the measurement of another, more accessible quantity. Precisely such a proxy, and part of the associated analysis, has already been developed in a different context: quantifying the rigidity of a fixed (inactive) conformation protein, KvAP— a voltage-gated potassium channel from *Aeropyrum Pernix* (23, 24). By providing both the remaining analysis and biological context, this perspective aims to assess the broader ramifications of such an indirect assay and its potential application for determining functional aspects of mechanically-gated channels. In doing so, concrete calculations are provided that not only demonstrate the required theory, but also provide results for experimental comparison.

The central idea is that measurements of a protein’s diffusion constant, D , as a function of applied membrane tension, σ , allow— via analysis— both conformational changes and effective physical properties, such as elastic moduli, to be determined. The relevant experimental setup is that of micropipette-aspirated single-particle tracking, as described in (24). This involves tracking (via “quantum dot” labelling) protein trajectories on the surface of a micropipette-aspirated Giant Unilamellar Vesicle (GUV) (see Fig. 1) where it is worth remarking that, in principle, the purification / reconstitution step might be made surfactant-free by employing co-polymner solvated nanodiscs (21, 22). In the context of mechanosensitive channels, analysing such data requires that energetic models of gating (25, 29–31) are combined with the classical hydrodynamics of (23), where the membrane is treated as two-dimensional low Reynolds number fluid. Here, a protein’s diffusion coefficient is calculated by first integrating the hydrodynamic stresses around the protein boundary to give the drag coefficient, λ , and then linking λ to D via the Stokes-Einstein relation (26).

The calculations presented here demonstrate that there are three very distinct D versus σ relations for three important classes of gating (25): *i*) dilation, where a cylindrically shaped channel opens by increasing its radius, *ii*) tilt, where opening is achieved by deforming from a truncated cone to a cylinder, and *iii*) a combination of both dilation and tilt. In the case of *i*), the membrane remains planar, and the formula of Saffman and Delbrück (SD) may be used, which also takes into account the extra drag induced by the three-dimensional embedding fluid. By contrast, applying the same protocol in the case of *ii*) leads to a calculation greatly complicated by geometry. Here, the conformation of the protein and the applied tension determine the shape of the membrane, which in turn affects the mobility of the protein via the mechanism of curvature-induced shear (23, 27, 28). This results in corrections to the SD expression, and an entirely different signature of gating. For case *iii*), which combines aspects of both pure dilation and pure tilt, the result is a surprisingly non-monotonic D versus σ curve.

The article concludes by discussing the advantages and disadvantages of micropipette-aspirated single-particle tracking as an indirect assay for the functional determination of mechanosensitive membrane proteins.

DILATION

As a cylindrically-shaped channel opens via dilation, its diffusion constant, D , decreases, due to the increase in the protein’s radius, a . This can be seen from the SD

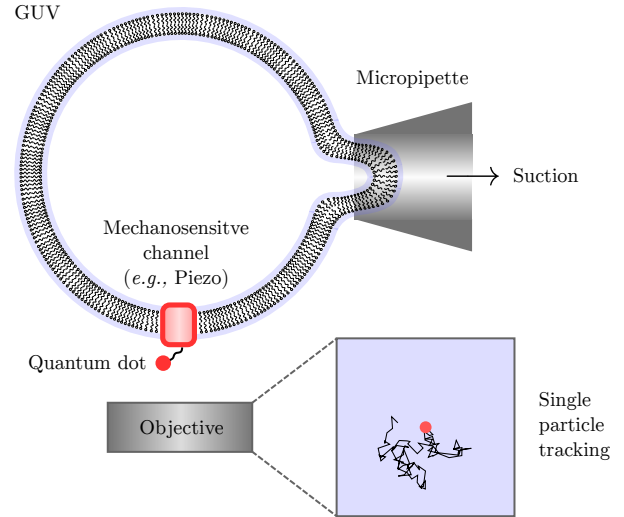


Figure 1: Schematic of single particle tracking on the surface of a micropipette aspirated GUV. As shown in (24), this setup can be used to obtain the diffusion constant, D , of a membrane channel, as a function of applied tension, σ . The resulting D vs. σ plots can be used to identify both the gating mechanism and elastic properties of mechanosensitive channels, such as the *Piezo* family of proteins.

formula,

$$D^{(SD)} = \frac{k_B T}{4 \pi \eta} \left[\log \left(\frac{\eta}{\mu a} \right) - \gamma \right], \quad (1)$$

which treats the membrane as a two-dimensional fluid of viscosity η , embedded in a three-dimensional fluid of viscosity $\mu < \eta$ (both at low Reynolds number). Here, k_B is Boltzmann’s constant, γ is Euler’s constant, T is temperature, and the effects of vesicle curvature are neglected since the radius of a GUV (μm) greatly exceeds that of a membrane-protein (nm).

The relationship between protein radius, a , and membrane tension, σ , is given by the energetics of gating, assumed here to be that of “hydrophobic mismatch” (29–31). The approach characterises the free energy of the (static) membrane plus protein system with just two terms. The first term $\pi \mathcal{K} (a - a_0) d^2$ arises from assigning a Hookean elastic energy to the lipids that border the protein, which either extend or compress their acyl chains (by an amount d) in order to match the “height” of the hydrophobic region on the exterior of the protein. Since experiments indicate the hydrophobic height decreases as a increases, a simple volume conserving model is adopted, implying $d = a_0^2 U / a^2$, where a_0 is just the lower bound on protein radius *i.e.*, $a \in [a_0, \infty)$. (The constant U is then just the extension of the lipid

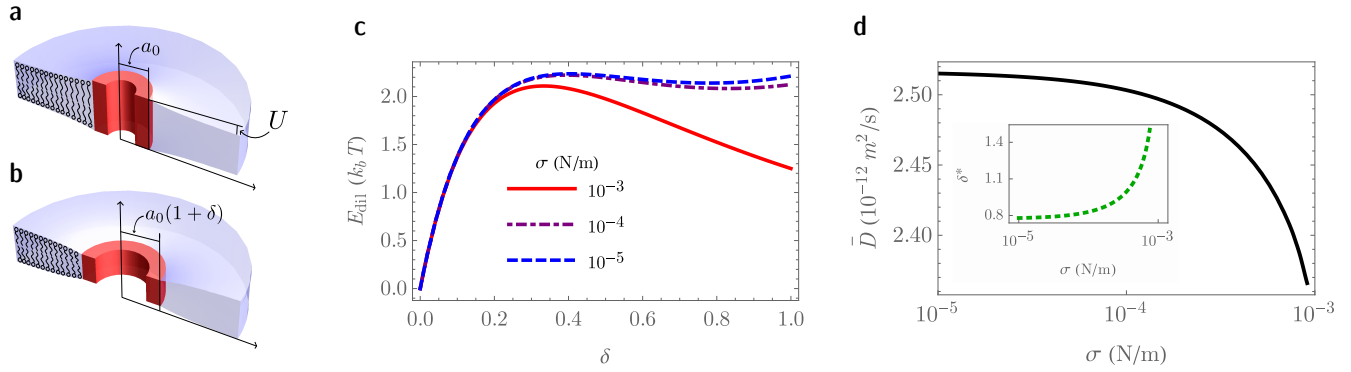


Figure 2: Gating by dilation. Panels (a) and (b) are cartoons of a dilation-gated protein channel in closed and open configurations, respectively. The diagrams indicate the extension (or compression) of the lipid acyl chains in the vicinity of the protein, giving rise to the gating energetics shown in panel (c). Irrespective of tension, the closed configuration corresponds to $\delta = 0$, whilst the open configuration (*i.e.*, the local nonzero minima δ^*) is both increasingly stable and occurs at greater dilations [inset of panel (d)], as applied tension is increased. Panel (d) plots the time average of the diffusion constant for a gating protein in thermal equilibrium (at room temperature) as a function of applied tension. The decrease of \bar{D} at higher tensions is due to open configurations having larger radii and being more stable.

acyl chains when $a = a_0$). The second term arises from the competition between the elastic deformation of the channel and the surface tension $\pi(k - \sigma)(a - a_0)^2$. Up to an additive constant, the combined energy is given by¹

$$E_{\text{dil}} = \frac{\pi \mathcal{K} a_0 \delta U^2}{(1 + \delta)^4} + \pi(k - \sigma) a_0^2 \delta^2, \quad (2)$$

which has been written using a dimensionless dilation $\delta = (a/a_0) - 1$. Estimates for \mathcal{K} , U and a_0 can all be taken from the literature (see Numerical Values section), whilst the elastic constant k is chosen to be the minimum value which ensures that (2) is bounded for all physically plausible tensions $\sigma < 10^{-3}$ N/m (the membrane of a GUV is known to tear at tensions of around 10^{-3} N/m). Imposing the constraint $\partial E_{\text{dil}}/\partial \delta = 0$ gives rise to two minima, located at $\delta = 0$ and $\delta = \delta^*(\sigma)$, which are taken as “closed” and “open” states, respectively. A schematic of these states is depicted in Figs. 2(a) and 2(b), whilst Fig. 2(c) and the inset of Fig. 2(d) demonstrate that the position and depth of the local minimum increases with applied tension.

Assuming that the channel is in equilibrium with the environment, the average rate at which thermal fluctuations cause the channel to open is just the escape rate, $R_{\delta=0}$, from the energy minimum at $\delta = 0$, and is given by Kramer’s formula (32, 33): $R = \mathcal{C} \exp[-E_{\text{barrier}}/k_B T]$, where \mathcal{C} is a constant and $E_{\text{barrier}} = \max_{\delta \in [0, \delta^*]} E(\delta)$. Similarly, the rate at

¹Notice that, rather than invoke a term corresponding to steric hindrance at small radii, it suffices to only consider energies greater than some value $E(0)$, since $\delta = 0$ is always a global minimum of the function, by construction.

which fluctuations cause the channel to close, $R_{\delta=\delta^*}$, is given by $R_{\delta=\delta^*} = \mathcal{C} \exp[-(E_{\text{barrier}} - E(\delta^*))/k_B T]$. The ratio of these rates is just the ratio of mean first passage times for traversing the energy barrier. Therefore, over long times, the fraction of time spent at $\delta = 0$ and $\delta = \delta^*$ approaches $1/[1 + \exp(-\Delta E/k_B T)]$ and $1/[1 + \exp(\Delta E/k_B T)]$, respectively, where $\Delta E = E(\delta^*) - E(0)$. The effective diffusion constant, \bar{D} , is calculated by substituting $\delta = 0$ and $\delta = \delta^*$ into (1) and then taking an average, weighted by the aforementioned time fractions. The result [Fig. 2(d)] indicates that the diffusion constant of a dilation-gated channel decreases with applied tension, but only on a small scale ($\sim 10^{-13}$ m²/s over three orders of magnitude of σ).

TILT

In contrast to gating via dilation, gating via tilt involves channels in the shape of a truncated cone, which deform the membrane in the vicinity of the protein [see Figs. 3(a) and 3(b)] and lead to corrections to (1). This is an example of so-called curvature-induced shear: the phenomenon whereby Gaussian curvature of the membrane modifies shear and hence drag and diffusion (23, 27, 28).

In order to calculate such corrections, it is therefore necessary to calculate the membrane shape induced by the channel. In principle, this shape not only depends on the conformation of the channel, but also its motion. That is, a non-zero channel velocity results in a spatially varying two-dimensional pressure (*i.e.*, tension), as well

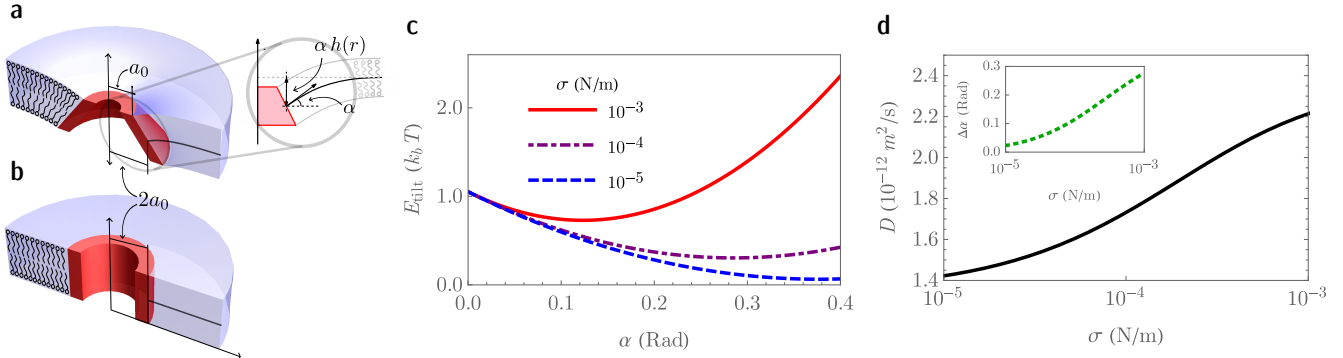


Figure 3: Gating by tilt. Panels (a) and (b) are cartoons of a tilt-gated protein channel at low and high tensions, respectively. The energy of the protein as a function of tilt angle α [panel (c)] has a single minima, α^* , where the torque due to applied tension is balanced by the protein’s torsional rigidity. As tension, σ , is increased, α^* decreases and the channel becomes increasingly cylindrical. Panel (d) shows that the diffusion constant of a tilt-gated protein increases with tension. This is because the large tilt-angles which correspond to low tensions imply a large curvature-induced shear, and hence low mobility. At higher tensions, the diffusion constant saturates as the protein becomes effectively cylindrical. The inset of panel (d) demonstrates that the protein undergoes substantial angular strains across the range of experimentally accessible tensions.

as a rotation-inducing torque on the channel, breaking the angular symmetry of deformations. However, in practice, since the drag itself is the leading order coefficient in a power series expansion of force in terms of velocity, such effects can be neglected when calculating λ , and the symmetric, equilibrium, shape suffices. Here, the equilibrium mid-surface, denoted \mathcal{S} , is calculated by minimising a Helfrich-like free energy functional (34),

$$E_{\text{mem}} = \int_{\mathcal{S}} (2\kappa H^2 + \bar{\kappa} K + \sigma) dA, \quad (3)$$

which describes a bilayer under surface tension σ that also has a bending energy (per unit area) of $2\kappa H^2 + \bar{\kappa} K$, where κ and $\bar{\kappa}$ are constant bending moduli and H and K are the mean and Gaussian curvatures, respectively. Using a small angle approximation, the solution to the corresponding Euler-Lagrange equation can be characterised by an axisymmetric height field $\alpha h(r)$, $\forall r \in [a, \infty)$, where α is the tilt-angle, subtended at the “walls” where the channel meets the membrane, and the function h is given by (23, 35)

$$h(r) = \frac{\ell K_0(r/\ell)}{K_1(a/\ell)}. \quad (4)$$

Here, K_n represents an order- n modified Bessel function of the second kind and the characteristic length scale is given by $\ell = \sqrt{\kappa/\sigma}$. The boundary terms of the same calculation yield the torque applied at the channel walls, between the membrane and protein (36)

$$\tau = 2\pi \alpha (a \sigma h(a) - \bar{\kappa}), \quad (5)$$

which is assumed to be hinged about the mid-plane of the membrane [see Figs. 3(a) and 3(b)]. If a conformation is to be stable, (5) must be balanced by the protein’s torsional rigidity, implying that the gating energy takes the form

$$E_{\text{tilt}} = \pi [\sigma a h(a) + \bar{\kappa}] \alpha^2 - \frac{k'}{2} \alpha^2 + [\tau_{\text{ref}}(\sigma_{\text{ref}}) - k' \alpha_{\text{ref}}] \alpha, \quad (6)$$

where the first term can be deduced from (5), the second term has the form of a torsion spring with rigidity k' , and the third term is just the known net torque at some reference angle, α_{ref} , and reference tension, σ_{ref} . By analogy with the case of dilation, the relationship between α and σ is provided by imposing $\partial E_{\text{tilt}}/\partial \alpha = 0$. This leads to a single minimum, whose depth, and position, $\alpha = \alpha^*(\sigma)$, increase as applied tension decreases [Fig. 3(c)].

What remains is to calculate the diffusion constant, where the standard approach of classical hydrodynamics may be used, *i.e.*, by solving the equations of incompressible Stokes flow in order to calculate the drag and then invoking the Stokes-Einstein relation. However, due to the geometry of the membrane, the hydrodynamics must now be formulated in a covariant way. That is, local quantities are expressed in the tangent plane of the membrane mid-surface \mathcal{S} [*i.e.*, defined by $\alpha^* h(r)$]. In general, such covariant Stokes equations are very hard to solve in all but a handful of special cases. However, in this case, the small size of angle α^* may be exploited, and therefore approximate solutions can be obtained as power series in α^* . This type of perturbative scheme is explained in detail in (23) (and the associated supplementary material), where the covariant Stokes flow

problem is solved by moving to a description in terms of a scalar stream function. After separating-out the angular dependence, the result is a scheme of fourth-order ODEs and boundary conditions, each of which corresponds to the radial part of a single coefficient in the perturbative expansion of the stream function in terms of α^* . The zeroth order contribution is constructed so that the SD result is recovered as $\alpha^* \rightarrow 0$ where, since the characteristic membrane length scale ℓ is much less than the SD length η/μ (true for tensions $\sigma \geq 2 \times 10^{-7}$ N m $^{-1}$) the role of the embedding fluid may then be ignored in all higher order corrections. The next lowest order correction is at $(\alpha^*)^2$, since diffusion cannot depend of the sign of α^* due to the up/down symmetry of the membrane. Obtaining the coefficient of this correction involves solving the radial part of an inhomogeneous biharmonic equation, the particular solution of which must be computed numerically. Despite the lack of a closed form result, the numerics can still be used to calculate corrections to Cauchy stress tensor and therefore both the drag and diffusion constants. Without recapitulating the detailed calculation of (23), the result is that

$$D = D^{(\text{SD})} + (\alpha^*)^2 D^{(2)} + O[(\alpha^*)^4], \quad (7)$$

where the numerically calculated coefficient $D^{(2)}$ is independent of α^* but still relies on the both σ , $h(r)$, and its higher derivatives. The result is plotted in Fig. 3(d), and indicates that as tension increases, the angular strain and hence diffusion constant increases until saturation when the protein effectively becomes cylindrical. The heuristic is that low tensions imply large tilt-angles, and therefore membrane shapes with large Gaussian curvature at the boundary of the protein. Such large curvatures induce large shears in the fluid flow, increasing drag and reducing protein diffusion.

COMBINED DILATION AND TILT

The energetics of combined dilation and tilt is assumed to be the sum $E_{\text{dil+tilt}} = E_{\text{dil}} + E_{\text{tilt}}$, where the substitution $a = a_0(1 + \delta)$ has been made in E_{tilt} . The result is a function of both α and δ , which is minimised by the constraints $\partial E_{\text{dil+tilt}}/\partial \alpha = 0$ and $\partial E_{\text{dil+tilt}}/\partial \delta = 0$. Solving first for $\alpha^*(\delta, \sigma)$, substituting into $E_{\text{dil+tilt}}$, and plotting the result against δ gives rise to Fig. 4(a). As in the case of pure dilation, there are two minima, zero and $\delta^*(\sigma)$ which represent “closed” and “open” states, respectively. Taking the average of these values, weighted by the fraction of time that a protein in thermal equilibrium would spend in each state, gives rise to Figs. 4(b) and 4(b) inset. Here, the behaviour of the system can be characterised by roughly three regimes: *i*) Low tensions ($\sim 10^{-5}$ N/m), where the protein is

conical and the response of the system to increasing tension only gives rise to small decreases in α which, in order to accommodate the changing membrane shape, is compensated-for by small contractions in the channel radius. *ii*) Mid-range tensions ($\sim 10^{-4}$ N/m), where the channel radius is effectively constant, and the response to increasing tension is to reduce the tilt-angle causing the channel to become increasingly cylindrical. *iii*) High tensions ($\sim 10^{-3}$ N/m), where the tilt-angle is very small, and pure dilation is recovered, *i.e.*, increasing tension increases the radius of an essentially cylindrical channel.

The resulting diffusion constant is shown by the solid black line of Fig. 4(c), where the lines for pure dilation (dotted) and pure tilt (dashed) are also shown. For the case of “tilt + dilation”, at low tensions, the combined effects of decreasing tilt-angle and radial contraction almost cancel each other out leading to a very shallow, nearly flat, D vs. σ curve. In the mid-range of tensions, the curve begins to rise steeply, and resembles the pure tilt curve, shifted along the horizontal axis. Finally, at high tensions, the protein is almost cylindrical and therefore increasing the tension leads to pure dilation. The result is that the curve peaks and diffusion begins to decrease as tension increases [Fig. 4(c), magnified section].

DISCUSSION

The calculations in this article demonstrate that different types of gating can be adequately distinguished by their respective D versus σ plots. Moreover, given data, the approaches set out here could feasibly be used to predict effective elastic moduli, such as the torsional- or radial-rigidity, by curve fitting, as in (23). However, that study concerned KvAP in its inactive conformation, and although mechanical forces have been suggested to modulate the voltage at which gating occurs, the method is most relevant to *mechanosensitive* channels, such as the aforementioned Piezo family, for example, whose *function* is directly related to tension.

However, correctly applying such methods to real-world proteins presents certain challenges. For example, single-particle cryo-EM indicates that the shape of Piezo1 is akin to a “propeller” (16), thus breaking angular symmetry and greatly complicating the aforementioned calculations. Similarly, such proteins exhibit certain unique traits, such as relatively rapid rates of inactivation (1), for example. These features must either emerge from a full analysis, or be taken account-of by the gating energetics.

In the context of detailed crystallographic approaches, the methods proposed here should be

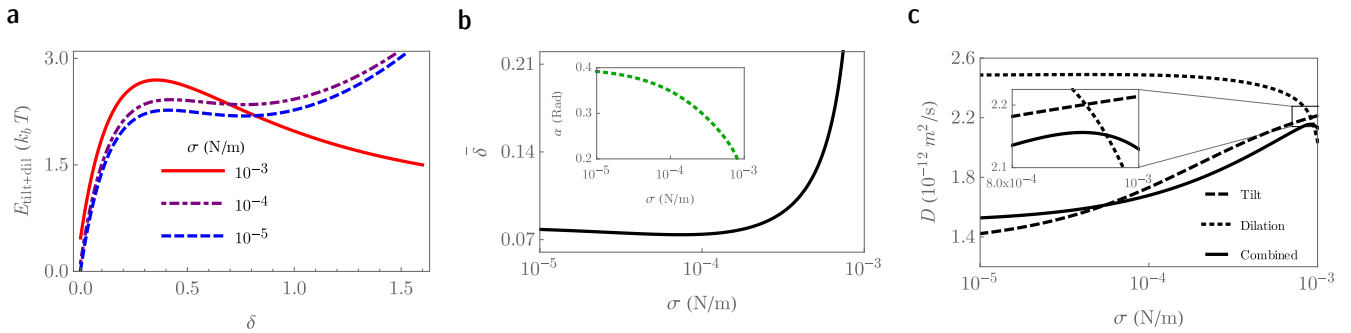


Figure 4: Gating by combined tilt and dilation. The energy has two minima, indicating distinct open and closed states [panel (a)]. The behaviour of the channel (both dilation and tilt) under applied tension is shown in panel (b), demonstrating the three regimes identified in the main text: *i*) tilt combined with contraction, *ii*) tilt dominated, and *iii*) dilation dominated. Panel (c) demonstrates the three unique signatures (D vs. σ plots) corresponding to pure dilation, pure tilt, and combined dilation and tilt. The magnified inset clarifies that the combined signature is non-monotonic at high tensions.

seen as a complimentary assay for investigating conformational changes in a coarse-grained way. That is, the approach overlooks complicated internal rearrangements, focussing instead on a channel's *effective* shape and *effective* elastic properties. Indeed, since only a diffusion coefficient needs to be measured, some of the technical issues associated with structural data may be sidestepped: neither crystallization nor chemical modification of the channel are required, and elastic moduli can be estimated directly by fitting gating models to the data. We note that the experimental accuracy of measuring diffusion coefficients via repeated single-particle tracking is around $\pm 0.1 \times 10^{-12} \text{ m}^2/\text{s}$ (24), and therefore properly resolving different gating mechanisms requires, as a minimum, gathering data over tensions ranging three orders of magnitude. Furthermore, the interesting features of combined gating occur at very high tensions (*circa* $10^{-3} \text{ m}^2/\text{s}$), above which bi-layer membranes are known to tear. Indeed, such issues notwithstanding, the approach still relies on a judicious choice of model for fitting and therefore, ideally, information from both coarse-grained and crystallographic approaches should be *combined* in order to fully understand membrane channel gating.

Going forwards, although this perspective argues that such techniques offer great promise, more work is clearly needed in order to refine certain aspects, both in the presence and absence of crystallographic data. Possible extensions may include the effects of membrane composition and annular lipid-protein interactions, or membrane curvature, neither of which were considered here. It is also worth remarking that, so far, proteins have only been treated in isolation, which is achieved experimentally by using very low concentrations. However, in the cell, concentrations of membrane-bound

proteins are likely to be much higher, leading to cooperative gating effects, such as those described in (38). One might speculate that such behaviour translates into spatial correlations between particle trajectories and hence modifications to diffusion and its corresponding D versus σ signature. Finally, it may also be possible to measure the functional response of a channel alongside its diffusion coefficient. That is, to monitor pH changes, or trans-membrane potentials, in order provide evidence that a channel is working or not. Either way, further work in the area is welcome.

NUMERICAL VALUES

The hydrodynamic viscosity of the membrane ($\eta = 6 \times 10^{-10} \text{ kg s}^{-1}$) and surrounding fluid ($\mu = 10^{-3} \text{ kg m}^{-1} \text{ s}^{-1}$) were taken from (24). The minimum channel radius ($a_0 = 2 \times 10^{-9} \text{ m}$), maximum acyl-chain extension ($U = 10^{-10} \text{ m}$), and corresponding spring constant ($\mathcal{K} = 4 \times 10^9 \text{ J}$), were taken from (30). The elastic moduli of the lipid bilayer ($\kappa = 20 k_B T$, and $\bar{\kappa} = 0.9 \kappa$, for $T = 298 \text{ K}$) were taken from (37). The torsional rigidity ($k' = 100 k_B T$) was taken to match the order of magnitude of the voltage-gated channel KvAP (23). Dilational rigidity ($k = 10^{-3} \text{ J m}^{-2}$) was chosen to be the minimum value that ensured the energy was bounded for tensions below 10^{-3} N m^{-1} . Similarly, the reference tilt angle ($\alpha_{\text{ref}} = 0.4 \text{ Rad}$) at very low tension ($\sigma_{\text{ref}} = 10^{-8} \text{ N m}^{-1}$) was chosen to correspond to the maximum tilt found in KvAP (23).

ACKNOWLEDGMENTS

The author acknowledges both comments from and discussions with: Prof. M. S. Turner (Warwick, United Kingdom), Prof. M. Rao (NCBS, India), Dr. A. Rautu (NCBS, India), and

K. Husain (NCBS, India). The author thanks the Tata Institute for Fundamental Research (India) and the Simons Foundation (USA) for financial support.

References

- [1] Coste, B., J. Mathur, M. Schmidt, T. J. Earley, S. Ranade, M. J. Petrus, A. E. Dubin, A. Patapoutian, 2011. Piezo1 and Piezo2 are essential components of distinct mechanically-activated cation channels. *Science* 330:55–60.
- [2] Coste, B., B. Xiao, J. S. Santos, R. Syeda, J. Grandl, K. S. Spencer, S. E. Kim, M. Schmidt, J. Mathur, A. E. Dubin, M. Montal, and A. Patapoutian, 2012. Piezo proteins are pore-forming subunits of mechanically activated channels. *Nature* 483:176–181.
- [3] Kim, S. E., B. Coste, A. Chadha, B. Cook, and A. Patapoutian, 2012. The role of Drosophila Piezo in mechanical nociception. *Nature* 483:209–212.
- [4] Woo, S.-H., S. Ranade, A. D. Weyer, A. E. Dubin, Y. Baba, Z. Qiu, M. Petrus, T. Miyamoto, K. Reddy, E. A. Lumpkin, C. L. Stucky, and A. Patapoutian, 2014. Piezo2 is required for Merkel-cell mechanotransduction. *Nature* 509:622–626.
- [5] Ranade, S. S., Z. Qiu, S.-H. Woo, S. S. Hur, S. E. Murthy, S. M. Cahalan, J. Xu, J. Mathur, M. Bandell, B. Coste, Y.-S. J. Li, S. Chien, and A. Patapoutian, 2014. Piezo1, a mechanically activated ion channel, is required for vascular development in mice. *Proc. Natl. Acad. Sci.* 111:10347–10352.
- [6] Ranade, S. S., S.-H. Woo, A. E. Dubin, R. A. Moshourab, C. Wetzel, M. Petrus, J. Mathur, V. Bégay, B. Coste, J. Mainquist, A. J. Wilson, A. G. Francisco, K. Reddy, Z. Qiu, J. N. Wood, G. R. Lewin, and A. Patapoutian, 2014. Piezo2 is the major transducer of mechanical forces for touch sensation in mice. *Nature* 516:121–125.
- [7] Cahalan, S. M., V. Lukacs, S. S. Ranade, S. Chien, M. Bandell, and A. Patapoutian, 2015. Piezo1 links mechanical forces to red blood cell volume. *Elife* 4.
- [8] Woo, S.-H., V. Lukacs, J. C. de Nooij, D. Zaytseva, C. R. Criddle, A. Francisco, T. M. Jessell, K. A. Wilkinson, and A. Patapoutian, 2015. Piezo2 is the principal mechanotransduction channel for proprioception. *Nat. Neurosci.* 18:1756–1762.
- [9] Doyle, D. A., 1998. The Structure of the Potassium Channel: Molecular Basis of K⁺ Conduction and Selectivity. *Science* 280:69–77.
- [10] Jiang, Y., A. Lee, J. Chen, M. Cadene, B. T. Chait, and R. MacKinnon, 2002. Crystal structure and mechanism of a calcium-gated potassium channel. *Nature* 417:515–522.
- [11] Dutzler, R., E. B. Campbell, M. Cadene, B. T. Chait, and R. MacKinnon, 2002. X-ray structure of a Cl⁻ channel at 3.0 Å reveals the molecular basis of anion selectivity. *Nature* 415:287–294.
- [12] Jiang, Y., A. Lee, J. Chen, V. Ruta, M. Cadene, B. T. Chait, and R. MacKinnon, 2003. X-ray structure of a voltage-dependent K⁺ channel. *Nature* 423:33–41.
- [13] Gouaux, E., 2005. Principles of Selective Ion Transport in Channels and Pumps. *Science* 310:1461–1465.
- [14] Long, S. B., 2005. Crystal Structure of a Mammalian Voltage-Dependent Shaker Family K⁺ Channel. *Science* 309:897–903.
- [15] Doerr, A., 2015. Single-particle cryo-electron microscopy. *Nat. Methods* 13:23–23.
- [16] Ge, J., W. Li, Q. Zhao, N. Li, M. Chen, P. Zhi, R. Li, N. Gao, B. Xiao, and M. Yang, 2015. Architecture of the mammalian mechanosensitive Piezo1 channel. *Nature* 527:64–69.
- [17] Long, S. B., X. Tao, E. B. Campbell, and R. MacKinnon, 2007. Atomic structure of a voltage-dependent K⁺ channel in a lipid membrane-like environment. *Nature* 450:376–382.
- [18] Axford, D., J. Foadi, N.-J. Hu, H. G. Choudhury, S. Iwata, K. Beis, G. Evans, and Y. Alguel, 2015. Structure determination of an integral membrane protein at room temperature from crystals in situ. *Acta Crystallogr. Sect. D Biol. Crystallogr.* 71:1228–1237.
- [19] Huang, C.-Y., V. Olieric, P. Ma, E. Panepucci, K. Diederichs, M. Wang, and M. Caffrey, 2015. In meso in situ serial X-ray crystallography of soluble and membrane proteins. *Acta Crystallogr. Sect. D Biol. Crystallogr.* 71:1238–1256.
- [20] Moraes, I., G. Evans, J. Sanchez-Weatherby, S. Newstead, and P. D. S. Stewart, 2014. Membrane protein structure determination — The next generation. *Biochim. Biophys. Acta - Biomembr.* 1838:78–87.
- [21] Lee, S. C., T. J. Knowles, V. L. G. Postos, M. Jamshad, R. A. Parslow, Y.-P. Lin, A. Goldman, P. Sridhar, M. Overduin, S. P. Muench, and T. R. Dafforn, 2016. A method for detergent-free isolation of membrane proteins in their local lipid environment. *Nat. Protoc.* 11:7, 1149–1162.
- [22] Dörr, J. M., M. C. Koorengevel, M. Schäfer, A. V. Prokofyev, S. Scheidelaar, E. A. W. van der Cruisjen, T. R. Dafforn, M. Baldus, and J. A. Killian, 2014. Detergent-free isolation, characterization, and functional reconstitution of tetrameric K⁺ channel: The power of native nanodiscs. *Proc. Natl. Acad. Sci. USA* 111, 18607–18612.
- [23] Morris, R. G., and M. S. Turner, 2015. Mobility Measurements Probe Conformational Changes in Membrane Proteins due to Tension. *Phys. Rev. Lett.* 115:198101.
- [24] Quemeneur, F., J. K. Sigurdsson, M. Renner, P. J. Atzberger, P. Bassereau, and D. Lacoste, 2014. Shape matters in protein mobility within membranes. *Proc. Natl. Acad. Sci. U. S. A.* 111:5083–7.
- [25] Reeves, D., T. Ursell, P. Sens, J. Kondev, and R. Phillips, 2008. Membrane mechanics as a probe of ion-channel gating mechanisms. *Phys. Rev. E* 78:041901.
- [26] Batchelor, G. K., 1967. An introduction to fluid dynamics. Cambridge University Press, Cambridge, England.
- [27] Arroyo, M., and A. DeSimone, 2009. Relaxation dynamics of fluid membranes. *Phys. Rev. E* 79:031915.

- [28] Henle, M. L., and A. J. Levine, 2010. Hydrodynamics in curved membranes: The effect of geometry on particulate mobility. Phys. Rev. E 81:011905.
- [29] Wiggins, P., and R. Phillips, 2004. Analytic models for mechanotransduction: Gating a mechanosensitive channel. Proc. Natl. Acad. Sci. 101:4071–4076.
- [30] Wiggins, P., and R. Phillips, 2005. Membrane-Protein Interactions in Mechanosensitive Channels. Biophys. J. 88:880–902.
- [31] Phillips, R., T. Ursell, P. Wiggins, and P. Sens, 2009. Emerging roles for lipids in shaping membrane-protein function. Nature 459:379–385.
- [32] Gardiner, C., 1985. Handbook of stochastic methods. Springer-Verlag, Berlin.
- [33] van Kampen, N. G., 1992. Stochastic processes in physics and chemistry. Elsevier, Amsterdam.
- [34] Helfrich, W., 1973. Elastic properties of lipid bilayers: theory and possible experiments. Z. Naturforsch. 28:693–703.
- [35] Weikl, T. R., M. M. Kozlov, and W. Helfrich, 1998. Interaction of conical membrane inclusions: Effect of lateral tension. Phys. Rev. E 57:6988–6995.
- [36] Morris, R. G., and M. S. Turner, 2016. Erratum: Mobility Measurements Probe Conformational Changes in Membrane Proteins due to Tension [Phys. Rev. Lett. 115 , 198101 (2015)]. Phys. Rev. Lett. 116:239901.
- [37] Hu, M., J. J. Briguglio, and M. Deserno, 2012. Determining the Gaussian Curvature Modulus of Lipid Membranes in Simulations. Biophys. J. 102:1403–1410.
- [38] Haselwandter, C. A., and R. Phillips, 2013. Directional interactions and cooperativity between mechanosensitive membrane proteins. Europhys. Lett. **101** 68002.